STATISTICAL DISTRIBUTION OF DETERMINANT OF POLARIMETRIC COVARIANCE MATRIX

Ken Yoong LEE and Timo Rolf BRETSCHNEIDER
Airbus Group Innovations Singapore
110 Seletar Aerospace View, Singapore 797562
Tel: +65 65927324; Fax: +65 66591276
Email: {kenyoong.lee, timo.bretschneider}@airbus.com

KEY WORDS: Synthetic aperture radar, texture model, generalised variance, Meijer G-function, ALOS PALSAR

ABSTRACT: This paper examines the use of standardised generalised variance for statistical modelling of forest clutter in ALOS PALSAR multilook L-band dual-polarisation (HH and HV) data. Its probability density functions (PDFs) under homogeneous model and texture model were obtained, where the PDFs can be expressed in terms of Meijer G-function. From the modelling results, the texture model was found to provide a better fitting compared with the homogeneous model.

1. INTRODUCTION

In multivariate statistics, generalised variance refers to the determinant of p-dimensional covariance matrix (Kocherlakota and Kocherlakota 1983; Anderson 2003, Chapter 7). Its positive p-th root is known as standardised generalised variance (SenGupta 1987a, 1987b, 2006). Since its first introduction by Wilks (1932, Section 3), the generalised variance has been considered as a measure of the spread of observations or overall variability (Goodman 1968; Rencher and Christensen 2012, pp. 81–82). The central and noncentral distributions of the generalised variance were derived from real Wishart distribution by Bagai (1962, 1965), Consul (1964), Mathai and Rathie (1971), Mathai (1972). The complex analogues of their results, which were obtained from complex Wishart distribution, appeared in Goodman (1963), Gupta and Rathie (1983), Zhu *et al*. (2009).

Statistical modelling of radar clutter has received a considerable amount of attention in the literature. Among some relevant works are Yueh *et al*. (1991), Anastassopoulos *et al*. (1999), Sayama and Sekine (2002), Moser *et al*. (2006), Bian and Mercer (2014). In our previous papers (Lee and Bretschneider 2013, 2015), the so-called trace statistic was explored for modelling sea clutter and terrain clutter in multilook polarimetric synthetic aperture radar (SAR) data. The trace statistic is also applicable for single-look polarimetric SAR data, where it becomes squared radius in this case. Apart from the trace statistic, it is of particular interest to investigate another statistical measure, namely standardised generalised variance, for statistical modelling of radar clutter.

This paper presents our modelling work of forest clutter in ALOS PALSAR multilook dual-polarisation data by using standardised generalised variance. The ALOS PALSAR data are described in Section 2. Sections 3 and 4 focus separately on the standardised generalised variance under homogeneous model and texture model. The forest clutter modelling results are discussed in Section 5. Finally, conclusions are drawn in Section 6.

2. ALOS PALSAR DATA

For this study, nine sets of ALOS PALSAR single-look complex data (level 1.1) were downloaded via Vertex from the Alaska Satellite Facility (https://vertex.daac.asf.alaska.edu/). All the nine fine beam dual-polarisation (HH and HV) data were collected on the ascending orbit. Table 1 provides further information about the multitemporal datasets, which covered the same area of the South-East Pahang Peat Swamp Forest in the east coast of Peninsular Malaysia.

Table 1: Specifications of ALOS PALSAR test data

Scene identifier	Acquisition date (day/month/year)	Incidence angle at scene centre (°)	Faraday rotation (°)	Azimuth spacing (meter)
ALPSRP075210050	23/06/2007	38.745	-0.15	3.1848579
ALPSRP081920050	08/08/2007	38.765	-0.33	3.1914091
ALPSRP088630050	23/09/2007	38.757	-0.26	3.1848079
ALPSRP122180050	10/05/2008	38.760	-0.15	3.1846020
ALPSRP128890050	25/06/2008	38.754	-0.17	3.1912686
ALPSRP142310050	25/09/2008	38.750	-0.32	3.1848617
ALPSRP236250050	01/07/2010	38.760	-0.29	3.1846684
ALPSRP242960050	16/08/2010	38.758	-0.65	3.1914926
ALPSRP249670050	01/10/2010	38.756	-0.69	3.1846099

There were two SAR image files, one SAR leader file, one volume directory file, and one trailer file in each dataset. The number of range and azimuth pixels in the SAR image was 4640 and 18432, respectively. From the data set summary record in the leader file, the range pixel spacing was found to be 9.3685143 meters. The azimuth pixel spacing is, as tabulated in Table 1, about three times smaller than the range pixel spacing.

In the ALOS PALSAR single-look slant range dual-polarisation (HH and HV) data, each pixel can be represented by a two-dimensional complex vector

$$\mathbf{s} = c\begin{bmatrix} I_{\mathrm{HH}} + jQ_{\mathrm{HH}} \\ I_{\mathrm{HV}} + jQ_{\mathrm{HV}} \end{bmatrix} = \begin{bmatrix} s_{\mathrm{HH}} \\ s_{\mathrm{HV}} \end{bmatrix} \tag{1}$$

where $j = \sqrt{-1}$. The 32-bit in-phase and quadrature components of a pixel are denoted separately by I and Q. The scalar c is equal to $10^{(\mathrm{CF}-32)/20}$, where the calibration factor (CF) can be retrieved from the radiometric data record in the leader file. Since the azimuth spacing of the ALOS PALSAR single-look data is smaller than the range spacing, multilooking can then be performed by taking L neighbouring pixels in the azimuth direction for computing polarimetric covariance matrix:

$$\mathbf{C} = \frac{1}{L}\sum_{i=1}^{L} \mathbf{s}_i \mathbf{s}_i^{*\mathrm{T}} = \begin{bmatrix} \left\langle s_{\mathrm{HH}} s_{\mathrm{HH}}^{*} \right\rangle & \left\langle s_{\mathrm{HH}} s_{\mathrm{HV}}^{*} \right\rangle \\ \left\langle s_{\mathrm{HH}}^{*} s_{\mathrm{HV}} \right\rangle & \left\langle s_{\mathrm{HV}} s_{\mathrm{HV}}^{*} \right\rangle \end{bmatrix}. \tag{2}$$

The superscripts $*$ and T denote the complex conjugate and transpose, respectively. The angle brackets $\langle . \rangle$ refer to the expectation. In the 2×2 Hermitian covariance matrix **C**, each diagonal element (also known as variance) is actually the backscattering coefficient or sigma-nought (σ^0) for different polarisations. The sigma-nought of HH polarisation, for example, can be calculated in decibel (dB) as

$$\sigma_{\mathrm{HH}}^{0}(\mathrm{dB}) = 10\log_{10}\left\langle s_{\mathrm{HH}} s_{\mathrm{HH}}^{*} \right\rangle = 10\log_{10}\left\langle I_{\mathrm{HH}}^2 + Q_{\mathrm{HH}}^2 \right\rangle + \mathrm{CF} - 32. \tag{3}$$

The phase difference between HH and HV polarisations is embedded in the off-diagonal elements.

3. STANDARDISED GENERALISED VARIANCE UNDER HOMOGENEOUS MODEL

Under the homogeneous model, the polarimetric covariance matrix **C** is assumed to follow a bivariate (p = 2) scaled central complex Wishart distribution ($L \geq p$):

$$f(\mathbf{C}) = \frac{L^{Lp}}{\Gamma_p(L)} |\mathbf{\Sigma}|^{-L} |\mathbf{C}|^{L-p} \exp\{-L\,\mathrm{tr}(\mathbf{\Sigma}^{-1}\mathbf{C})\}. \tag{4}$$

The notations | . | and tr represent separately the matrix determinant and trace. $\Gamma_p(.)$ refers to the complex multivariate gamma function and $\mathbf{\Sigma}$ is the population covariance matrix. The PDF of the standardised generalised variance under the homogeneous model for p = 2 is given by

$$f(\sqrt{|\mathbf{C}|}) = \frac{4L^{2L-1}}{\Gamma(L-1)\,\Gamma(L)} |\mathbf{\Sigma}|^{1/2-L} |\mathbf{C}|^{L-1} K_1\left(2L\sqrt{\frac{|\mathbf{C}|}{|\mathbf{\Sigma}|}}\right), \tag{5}$$

where $\Gamma(.)$ denotes the gamma function and $K_v(.)$ is the modified Bessel function of second kind with an order of v. By using the relation

$$\mathrm{G}_{02}^{20}\left(x \,\middle|\, \begin{matrix} - \\ a, b \end{matrix}\right) = 2\,x^{(a+b)/2} K_{a-b}(2\sqrt{x}), \tag{6}$$

the PDF in (5) can be written in terms of Meijer G-function as

$$f(\sqrt{|\mathbf{C}|}) = \frac{2L^2}{\Gamma(L-1)\,\Gamma(L)} \frac{\sqrt{|\mathbf{C}|}}{|\mathbf{\Sigma}|} \mathrm{G}_{02}^{20}\left(L^2 \frac{|\mathbf{C}|}{|\mathbf{\Sigma}|} \,\middle|\, \begin{matrix} - \\ L-2, L-1 \end{matrix}\right). \tag{7}$$

For more details on the Meijer G-function, the reader is referred to Erdélyi *et al*. (1953), Luke (1969), Mathai (1970), Mathai and Saxena (1973), Prudnikov *et al*. (1990), Andrews (1998), Gradshteyn and Ryzhik (2015). As shown in Appendix A, the first and second moments of the standardised generalised variance (p = 2) are separately

$$E(\sqrt{|\mathbf{C}|}) = \frac{\Gamma(L-\frac{1}{2})\,\Gamma(L+\frac{1}{2})}{\Gamma(L-1)\,\Gamma(L+1)} \sqrt{|\mathbf{\Sigma}|} \tag{8}$$

and

$$E(|\mathbf{C}|) = |\mathbf{\Sigma}|\,(L-1)/L. \tag{9}$$

The symbol $E(.)$ represents the expected value. It is noted here that $|\mathbf{\Sigma}|$ in (7) can be estimated from the first moment.

4. STANDARDISED GENERALISED VARIANCE UNDER TEXTURE MODEL

According to the texture model proposed by Lee *et al*. (1994), the polarimetric covariance matrix **C** is modulated by a scalar texture component *t*:

$$\widetilde{\mathbf{C}} = t\,\mathbf{C}. \tag{10}$$

The scalar texture component, which is a real positive random variable, is assumed to be gamma-distributed as

$$f(t) = \frac{\alpha^{\alpha}}{\Gamma(\alpha)} t^{\alpha-1} \exp(-\alpha t). \tag{11}$$

It has a unit mean, i.e. $E(t) = 1$, and its second moment is given by $E(t^2) = (\alpha+1)/\alpha$. Hence, its variance follows straightforwardly that $\mathrm{var}(t) = E(t^2) - [E(t)]^2 = 1/\alpha$. As derived in Appendix B, the PDF of the standardised generalised variance under the gamma texture model ($p = 2$) is given by

$$f(\sqrt{|\widetilde{\mathbf{C}}|}) = \frac{2(L\alpha)^{\alpha-1}}{\sqrt{\pi}\,\Gamma(L-1)\,\Gamma(L)\,\Gamma(\alpha)} \frac{|\widetilde{\mathbf{C}}|^{\alpha/2-1}}{|\mathbf{\Sigma}|^{(\alpha-1)/2}} \mathrm{G}_{04}^{40}\left(\frac{L^2\alpha^2}{4} \frac{|\widetilde{\mathbf{C}}|}{|\mathbf{\Sigma}|} \middle| \begin{matrix} - \\ 1, \frac{1}{2}, L-\frac{\alpha}{2}-\frac{1}{2}, L-\frac{\alpha}{2}+\frac{1}{2} \end{matrix} \right). \tag{12}$$

Since both *t* and **C** are statistically independent, the first and second moments for the standardised generalised variance under the gamma texture model ($p = 2$) can be easily obtained as follows:

$$E(\sqrt{|\widetilde{\mathbf{C}}|}) = E(\sqrt{|t\,\mathbf{C}|}) = E(t\sqrt{|\mathbf{C}|}) = E(t)E(\sqrt{|\mathbf{C}|}) = E(\sqrt{|\mathbf{C}|}) = \frac{\Gamma(L-\frac{1}{2})\,\Gamma(L+\frac{1}{2})}{\Gamma(L-1)\,\Gamma(L+1)} \sqrt{|\mathbf{\Sigma}|} \tag{13}$$

and

$$E(|\widetilde{\mathbf{C}}|) = E(|t\,\mathbf{C}|) = E(t^2\,|\mathbf{C}|) = E(t^2)E(|\mathbf{C}|) = \frac{(\alpha+1)}{\alpha} \frac{(L-1)}{L} |\mathbf{\Sigma}|. \tag{14}$$

Apart from the gamma distribution, previous studies showed that the scalar texture component might also follow other statistical distributions (Frery *et al*. 1997; Delignon and Pieczynski 2002; Freitas *et al*. 2005):

1) If *t* is inverse gamma distributed as

$$f(t) = \frac{\alpha^{\alpha+1}}{\Gamma(\alpha+1)} t^{-\alpha-2} \exp(-\alpha/t) \tag{15}$$

with $E(t) = 1$ and $\mathrm{var}(t) = 1/(\alpha-1)$, then the PDF of the standardised generalised variance under the inverse gamma texture model ($p = 2$) is derived in Appendix C to be in the form

$$f(\sqrt{|\widetilde{\mathbf{C}}|}) = \frac{2\alpha^{\alpha}}{\sqrt{\pi}\,L^{\alpha}\Gamma(L-1)\,\Gamma(L)\,\Gamma(\alpha+1)} \frac{|\mathbf{\Sigma}|^{\alpha/2}}{|\widetilde{\mathbf{C}}|^{(\alpha+1)/2}} \mathrm{G}_{22}^{22}\left(\frac{4L^2}{\alpha^2} \frac{|\widetilde{\mathbf{C}}|}{|\mathbf{\Sigma}|} \middle| \begin{matrix} 0, \frac{1}{2} \\ L+\frac{\alpha}{2}-1, L+\frac{\alpha}{2} \end{matrix} \right). \tag{16}$$

Its first moment is identical to (13), while its second moment is given by

$$E(|\widetilde{\mathbf{C}}|) = \frac{\alpha}{(\alpha-1)} \frac{(L-1)}{L} |\mathbf{\Sigma}|. \tag{17}$$

2) If *t* is inverted beta distributed as

$$f(t) = \frac{\Gamma(2\alpha+1)}{\Gamma(\alpha)\,\Gamma(\alpha+1)} t^{\alpha-1}(t+1)^{-2\alpha-1} \tag{18}$$

with $E(t) = 1$ and $\mathrm{var}(t) = 2/(\alpha-1)$, then the standardised generalised variance under the inverted beta texture model ($p = 2$) is shown in Appendix D to have the following PDF:

$$f(\sqrt{|\widetilde{\mathbf{C}}|}) = \frac{4^{\alpha}L^2}{\pi\,\Gamma(L-1)\,\Gamma(L)\,\Gamma(\alpha)\,\Gamma(\alpha+1)} \frac{\sqrt{|\widetilde{\mathbf{C}}|}}{|\mathbf{\Sigma}|} \mathrm{G}_{24}^{42}\left(\frac{L^2\,|\widetilde{\mathbf{C}}|}{|\mathbf{\Sigma}|} \middle| \begin{matrix} -\frac{\alpha}{2}-\frac{1}{2}, -\frac{\alpha}{2}-1 \\ \frac{\alpha}{2}-\frac{1}{2}, \frac{\alpha}{2}-1, L-2, L-1 \end{matrix} \right). \tag{19}$$

Its first moment is given by (13), while its second moment takes the form

$$E(|\widetilde{\mathbf{C}}|) = \frac{(\alpha+1)}{(\alpha-1)} \frac{(L-1)}{L} |\mathbf{\Sigma}|. \tag{20}$$

5. IMPLEMENTATION AND RESULTS

In this study three-look ($L = 3$) dual-polarization SAR data were formed for each scene, where the 2×2 polarimetric covariance matrix **C** was computed by using three pixels in the azimuth direction. The number of azimuth pixels reduced from 18432 to 6144 after multilooking. The value of calibration factor was –83 for all the nine scenes. Figure 1 shows the three-look colour composite images, where σ^0_{HH}, σ^0_{HV}, and $\sigma^0_{\mathrm{HV}}/\sigma^0_{\mathrm{HH}}$ are assigned to the red, green, and blue colour space. Being the longest river (about 459 km long) in Peninsular Malaysia, the Pahang River, which drains the water to the South China Sea, can be clearly seen in the figure. For statistical modelling, three regions of

peat swamp forest were chosen and extracted from each three-look dual-polarization SAR data. In Figure 1, the three regions are shown in yellow colour and are labelled A, B, and C, respectively. Table 2 lists the number of pixels for the selected regions, where each region contains more than 65000 pixels.

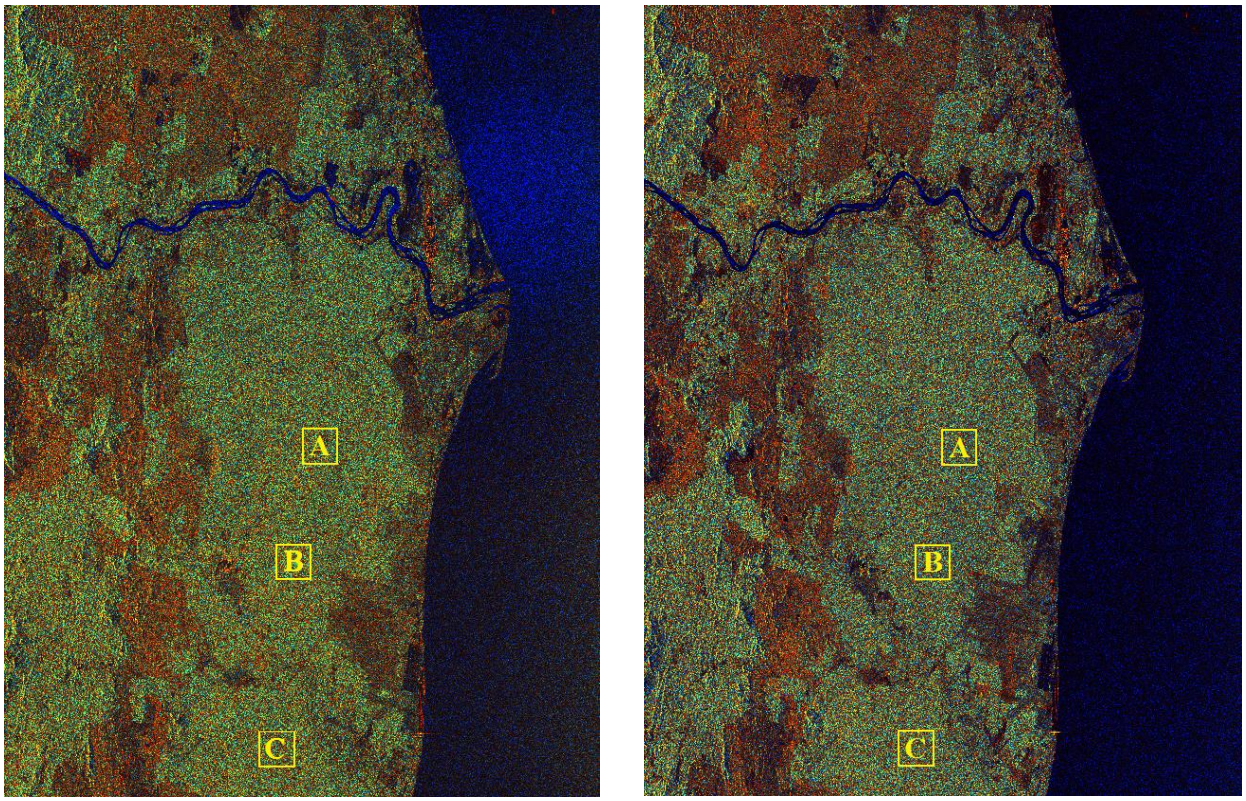

(a) (b)

Figure 1: Three-look colour composite images generated from ALOS PALSAR single-look fine beam dual-polarisation data, which were acquired on (a) 23rd June 2007 and (b) 25th June 2008. © JAXA/METI

Table 2: Number of pixels for selected regions of forest clutter

	Number of range pixels	Number of azimuth pixels	Total number of pixels
Forest A	253	265	67045
Forest B	255	259	66045
Forest C	258	266	68628

The forest clutter modelling was carried out based on the aforementioned standardised generalised variance, where both the homogeneous model and the texture model were considered. For each selected region of forest clutter, the following procedures were applied:

1. Compute the standardised generalised variance of each pixel.
2. Construct the histogram of the standardised generalised variance.
3. Compute the first and second moments of the standardised generalised variance.
4. Estimate the value of $|\boldsymbol{\Sigma}|$ from the first moment.
5. Plot the PDF of the standardised generalised variance under the homogeneous model onto the constructed histogram.
6. Estimate the alpha value from the second moment.
7. Plot the PDF of the standardised generalised variance under the texture model onto the constructed histogram.

It is important to note here that the PDF calculation was solved through numerical integration by using Simpson's rule. Moreover, the Meijer G-function, which is available in the Python mpmath library (http://mpmath.org/), was used in this study.

Table 3 lists the estimated alpha values of the gamma texture model. The range of the alpha values was between 9.0391 and 14.174. The smaller alpha value indicated that the texture component exhibited higher variance and hence the region of forest clutter was more heterogeneous. Figures 2 and 3 present the histograms of the standardised generalised variance, which were constructed from the selected regions of forest clutter. Visually, it is obvious in the figures that the texture model fits the histograms better than the homogeneous model.

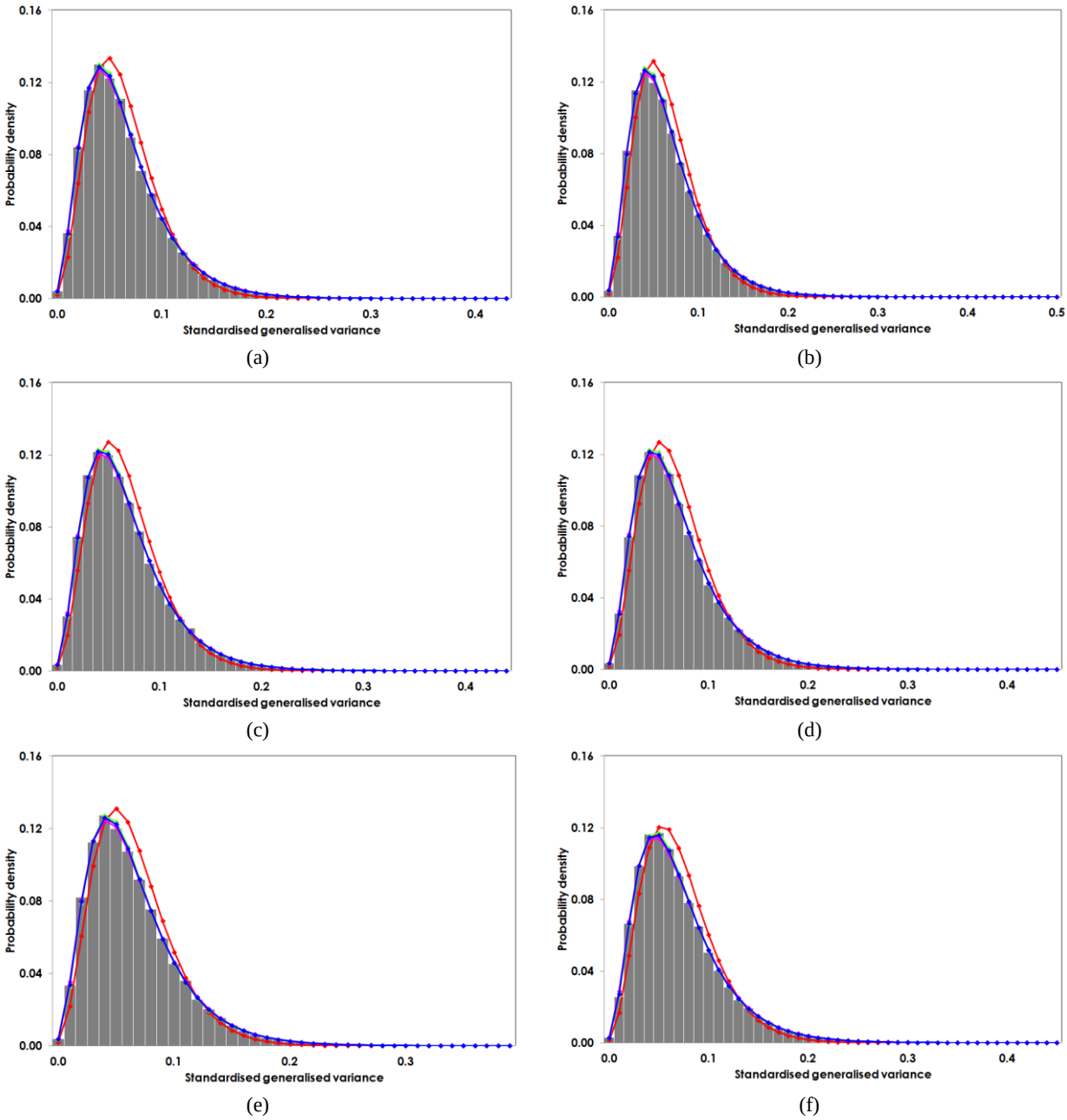

Figure 2: Histograms of the standardised generalised variance. On the left, (a), (c), and (e) are the histograms constructed separately from Forest A, Forest B, and Forest C in the ALOS PALSAR dual-polarisation data, which were acquired on 23rd June 2007. On the right, (b), (d), and (f) are the histograms constructed separately from Forest A, Forest B, and Forest C in the ALOS PALSAR dual-polarisation data, which were acquired on 23rd September 2007. The PDF of the standardised generalised variance under the homogeneous model is plotted in red colour. The magenta-coloured, blue-coloured, and green-coloured lines represent the PDFs of the standardised generalised variance under the gamma, inverted beta, and inverse gamma texture models, respectively.

Table 3: Alpha values for selected regions of forest clutter

Scene identifier	Forest A	Forest B	Forest C
ALPSRP075210050	12.8265	13.0244	12.9667
ALPSRP081920050	14.0481	14.1740	13.4478
ALPSRP088630050	13.4141	12.5391	12.4206
ALPSRP122180050	13.2066	13.0274	12.5062
ALPSRP128890050	10.3336	9.6960	9.0391
ALPSRP142310050	13.6860	13.0381	13.5867
ALPSRP236250050	12.5153	12.6010	12.2138
ALPSRP242960050	12.5467	12.9288	12.4968
ALPSRP249670050	11.3976	10.7420	11.1683

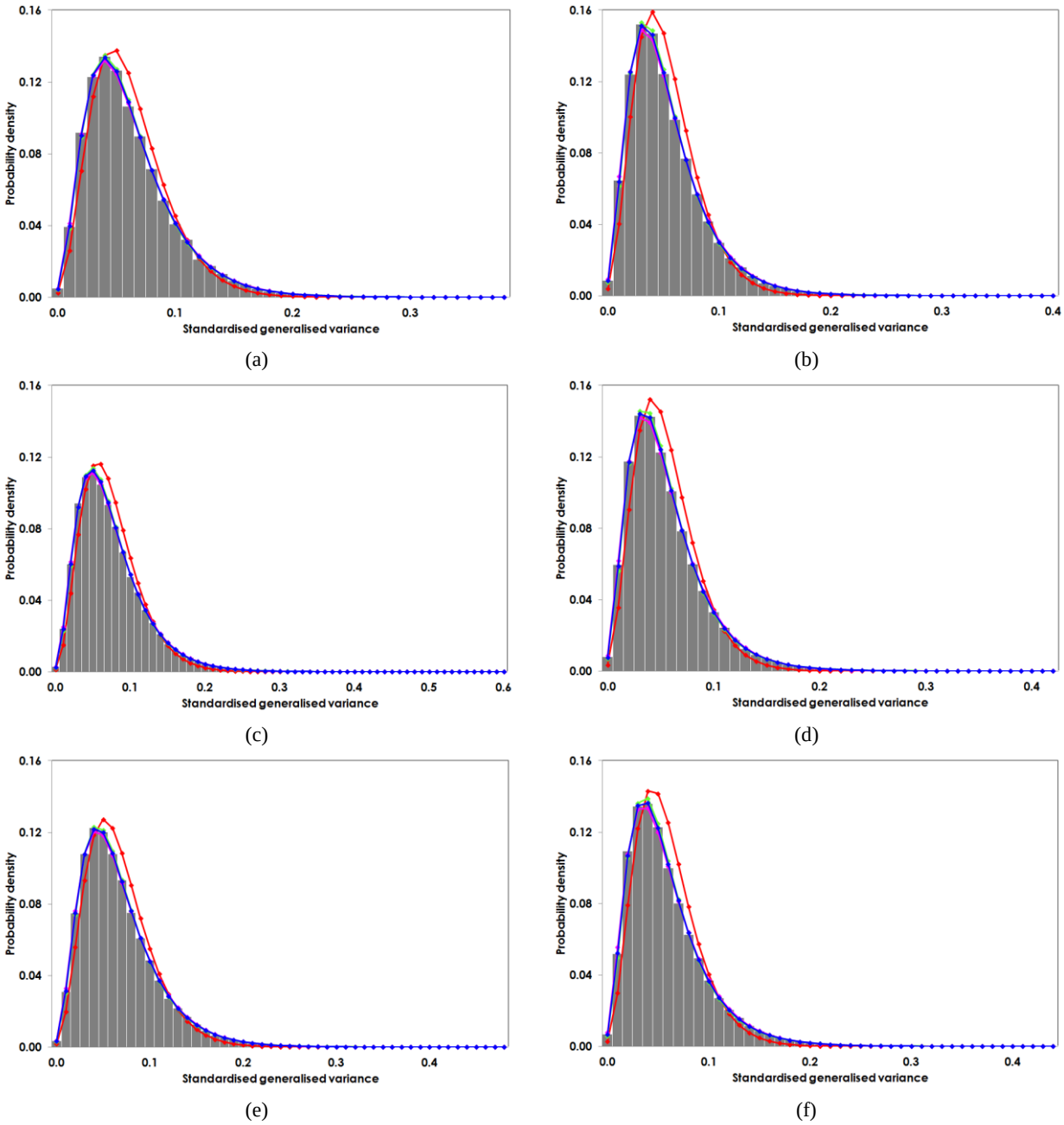

Figure 3: Histograms of the standardised generalised variance. On the left, (a), (c), and (e) are the histograms constructed separately from Forest A, Forest B, and Forest C in the ALOS PALSAR dual-polarisation data, which were acquired on 10th May 2008. On the right, (b), (d), and (f) are the histograms constructed separately from Forest A, Forest B, and Forest C in the ALOS PALSAR dual-polarisation data, which were acquired on 25th June 2008. The PDF of the standardised generalised variance under the homogeneous model is plotted in red colour. The magenta-coloured, blue-coloured, and green-coloured lines represent the PDFs of the standardised generalised variance under the gamma, inverted beta, and inverse gamma texture models, respectively.

In this study, the chi-squared test statistic was computed to further assess the goodness of fit. It is defined as

$$\chi^2 = \sum_{i=1}^{k} \frac{(O_i - E_i)^2}{E_i}, \tag{21}$$

where k is the number of bins. The observed frequency and the expected (or theoretical) frequency for bin i are denoted separately by O_i and E_i. A smaller value of the chi-squared test statistic indicates a better fitting result. Table 4 tabulates the computed chi-squared test statistics, where the number of bins used was 25. In Table 4, Homo represents the homogeneous model, while Gam, IB, and IGam refer separately to the gamma, inverted beta, and inverse gamma texture models. It is evident that the chi-squared test statistics were smaller for the texture model. The computed values confirmed that the texture model gave a better fitting compared with the homogeneous model. However, it is hard to identify the best texture model in this study. Although the inverted beta texture model outperformed others in many test cases for Forest B and Forest C, but the gamma texture model was found to fit better in some test cases for Forest A.

Table 4: Chi-squared test statistics for selected regions of forest clutter

Scene identifier	Forest A				Forest B				Forest C			
	Homo	Gam	IB	IGam	Homo	Gam	IB	IGam	Homo	Gam	IB	IGam
ALPSRP075210050	4662.6	36.9	**31.6**	53.5	4401.9	45.5	**38.7**	58.0	4932.8	30.3	**22.2**	41.9
ALPSRP081920050	3951.1	37.7	**34.2**	52.7	3590.4	**20.3**	23.5	46.4	4391.0	37.0	**17.7**	22.8
ALPSRP088630050	4147.4	**30.7**	35.9	65.2	4922.3	29.1	**16.8**	34.2	4826.4	59.2	**27.5**	29.5
ALPSRP122180050	4652.8	49.3	**45.1**	65.9	4200.4	**21.9**	23.6	50.0	4916.6	40.6	**20.5**	31.7
ALPSRP128890050	7390.6	39.0	**17.8**	49.7	8592.8	24.3	**17.4**	73.6	10179.2	49.9	**27.1**	88.9
ALPSRP142310050	4084.8	**21.9**	23.8	48.2	4139.6	**13.7**	25.6	60.3	4182.8	35.1	**28.2**	45.4
ALPSRP236250050	5270.9	**19.3**	24.2	58.4	4799.5	25.3	**21.5**	47.9	5579.2	**26.1**	43.9	92.1
ALPSRP242960050	4975.7	**32.3**	33.3	63.7	4532.8	36.1	**22.6**	37.3	5135.4	24.0	**23.6**	54.0
ALPSRP249670050	6106.8	**30.1**	30.4	69.1	6848.6	48.4	**36.8**	73.6	6556.0	26.1	**25.0**	66.0

6. CONCLUSIONS

In this paper the standardised generalised variance was studied, where its PDFs under the homogeneous model and the texture model can be expressed in terms of the Meijer G-function. Furthermore, the standardised generalised variance was applied for modelling peat swamp forest clutter in the ALOS PALSAR three-look dual-polarisation (HH and HV) data. Both the homogeneous model and the texture model were evaluated visually and quantitatively. The statistical modelling results revealed that the latter gave a better fitting compared with the former.

APPENDICES

A. Moments for Standardised Generalised Variance under Homogeneous Model

From (7), by letting $y = \sqrt{|\mathbf{C}|}$, the first moment is given by

$$E(\sqrt{|\mathbf{C}|}) = E(y) = \int_0^\infty y\, f(y)\, dy = \frac{2L^2}{\Gamma(L-1)\Gamma(L)|\mathbf{\Sigma}|} \int_0^\infty y^2\, \mathrm{G}_{02}^{20}\left(\frac{L^2}{|\mathbf{\Sigma}|} y^2 \,\middle|\, \begin{matrix} - \\ L-2, L-1 \end{matrix} \right) dy.$$

Let $z = y^2$, then $dz = 2\sqrt{z}\, dy$. Hence, we obtain

$$E(y) = \frac{L^2}{\Gamma(L-1)\Gamma(L)|\mathbf{\Sigma}|} \int_0^\infty \sqrt{z}\, \mathrm{G}_{02}^{20}\left(\frac{L^2}{|\mathbf{\Sigma}|} z \,\middle|\, \begin{matrix} - \\ L-2, L-1 \end{matrix} \right) dz = \sqrt{|\mathbf{\Sigma}|}\, \frac{\Gamma(L-\frac{1}{2})\Gamma(L+\frac{1}{2})}{\Gamma(L-1)\Gamma(L+1)}. \tag{22}$$

The above solution employs the following definite integral (Gradshteyn and Ryzhik 2015, p. 859):

$$\int_0^\infty x^{\rho-1}\, \mathrm{G}_{p\,q}^{m\,n}\left(\lambda x \,\middle|\, \begin{matrix} a_1, \ldots, a_p \\ b_1, \ldots, b_q \end{matrix} \right) dx = \lambda^{-\rho}\, \frac{\prod_{i=1}^{m} \Gamma(b_i + \rho) \prod_{i=1}^{n} \Gamma(1 - a_i - \rho)}{\prod_{i=m+1}^{q} \Gamma(1 - b_i - \rho) \prod_{i=n+1}^{p} \Gamma(a_i + \rho)}, \tag{23}$$

where an empty product is interpreted as unity. For the second moment, we have

$$E(y^2) = \frac{2L^2}{\Gamma(L-1)\Gamma(L)|\mathbf{\Sigma}|} \int_0^\infty y^3\, \mathrm{G}_{02}^{20}\left(\frac{L^2}{|\mathbf{\Sigma}|} y^2 \,\middle|\, \begin{matrix} - \\ L-2, L-1 \end{matrix} \right) dy$$

$$= \frac{L^2}{\Gamma(L-1)\Gamma(L)|\mathbf{\Sigma}|} \int_0^\infty z\, \mathrm{G}_{02}^{20}\left(\frac{L^2}{|\mathbf{\Sigma}|} z \,\middle|\, \begin{matrix} - \\ L-2, L-1 \end{matrix} \right) dz.$$

By using (23), we get

$$E(y^2) = \frac{|\mathbf{\Sigma}|\Gamma(L+1)}{L^2\Gamma(L-1)} = |\mathbf{\Sigma}|\frac{(L-1)}{L} = E(|\mathbf{C}|). \tag{24}$$

B. Probability Density Function of Standardised Generalised Variance under Gamma Texture Model

Under the gamma texture model, the texture component t is distributed as in (11) and the PDF of $\sqrt{|\mathbf{C}|}$ is given in (7). Since t and $\sqrt{|\mathbf{C}|}$ are statistically independent, their joint PDF is given by

$$f(t, \sqrt{|\mathbf{C}|}) = f(t)\, f(\sqrt{|\mathbf{C}|}) = \frac{2L^2\alpha^\alpha}{\Gamma(\alpha)\Gamma(L-1)\Gamma(L)} t^{\alpha-1} \frac{\sqrt{|\mathbf{C}|}}{|\mathbf{\Sigma}|} \exp(-\alpha t)\, \mathrm{G}_{02}^{20}\left(L^2 \frac{|\mathbf{C}|}{|\mathbf{\Sigma}|} \,\middle|\, \begin{matrix} - \\ L-2, L-1 \end{matrix} \right). \tag{25}$$

Let $u = t\sqrt{|\mathbf{C}|}$ and $v = t$, then the Jacobian of the transformation is $1/v$ and their joint PDF is

$$f(u,v) = \frac{2L^2\alpha^\alpha u}{\Gamma(\alpha)\,\Gamma(L-1)\,\Gamma(L)\,|\boldsymbol{\Sigma}|}\, v^{\alpha-3}\exp(-\alpha v)\,\mathrm{G}_{02}^{20}\left(\frac{L^2u^2}{|\boldsymbol{\Sigma}|\,v^2}\,\middle|\,\begin{matrix}-\\ L-2, L-1\end{matrix}\right). \tag{26}$$

The PDF of u can be obtained by integrating out v:

$$\begin{aligned} f(u) &= \frac{2L^2\alpha^\alpha u}{\Gamma(\alpha)\,\Gamma(L-1)\,\Gamma(L)\,|\boldsymbol{\Sigma}|}\int_0^\infty v^{\alpha-3}\exp(-\alpha v)\,\mathrm{G}_{02}^{20}\left(\frac{L^2u^2}{|\boldsymbol{\Sigma}|\,v^2}\,\middle|\,\begin{matrix}-\\ L-2, L-1\end{matrix}\right)dv \\ &= \frac{2L^2\alpha^\alpha u}{\Gamma(\alpha)\,\Gamma(L-1)\,\Gamma(L)\,|\boldsymbol{\Sigma}|}\int_0^\infty v^{\alpha-3}\exp(-\alpha v)\,\mathrm{G}_{20}^{02}\left(\frac{|\boldsymbol{\Sigma}|\,v^2}{L^2u^2}\,\middle|\,\begin{matrix}3-L, 2-L\\ -\end{matrix}\right)dv \\ &= \frac{2L^{\alpha-1}\alpha^\alpha u^{\alpha-2}}{\Gamma(\alpha)\,\Gamma(L-1)\,\Gamma(L)\,|\boldsymbol{\Sigma}|^{(\alpha-1)/2}}\int_0^\infty \exp(-\alpha v)\,\mathrm{G}_{20}^{02}\left(\frac{|\boldsymbol{\Sigma}|\,v^2}{L^2u^2}\,\middle|\,\begin{matrix}\frac{\alpha}{2}+\frac{3}{2}-L, \frac{\alpha}{2}+\frac{1}{2}-L\\ -\end{matrix}\right)dv \\ &= \frac{2L^{\alpha-1}\alpha^{\alpha-1}u^{\alpha-2}}{\sqrt{\pi}\,\Gamma(\alpha)\,\Gamma(L-1)\,\Gamma(L)\,|\boldsymbol{\Sigma}|^{(\alpha-1)/2}}\,\mathrm{G}_{40}^{04}\left(\frac{4|\boldsymbol{\Sigma}|}{L^2\alpha^2u^2}\,\middle|\,\begin{matrix}0, \frac{1}{2}, \frac{\alpha}{2}+\frac{3}{2}-L, \frac{\alpha}{2}+\frac{1}{2}-L\\ -\end{matrix}\right) \\ &= \frac{2L^{\alpha-1}\alpha^{\alpha-1}u^{\alpha-2}}{\sqrt{\pi}\,\Gamma(\alpha)\,\Gamma(L-1)\,\Gamma(L)\,|\boldsymbol{\Sigma}|^{(\alpha-1)/2}}\,\mathrm{G}_{04}^{40}\left(\frac{L^2\alpha^2u^2}{4|\boldsymbol{\Sigma}|}\,\middle|\,\begin{matrix}-\\ 1, \frac{1}{2}, L-\frac{\alpha}{2}-\frac{1}{2}, L-\frac{\alpha}{2}+\frac{1}{2}\end{matrix}\right). \end{aligned} \tag{27}$$

The above solution involves the use of the following identities (Gradshteyn and Ryzhik 2015, p. 1043):

$$\mathrm{G}_{p\,q}^{m\,n}\left(\frac{1}{x}\,\middle|\,\begin{matrix}a_1,\ldots,a_p\\ b_1,\ldots,b_q\end{matrix}\right) = \mathrm{G}_{q\,p}^{n\,m}\left(x\,\middle|\,\begin{matrix}1-b_1,\ldots,1-b_q\\ 1-a_1,\ldots,1-a_p\end{matrix}\right) \tag{28}$$

and

$$x^r\,\mathrm{G}_{p\,q}^{m\,n}\left(x\,\middle|\,\begin{matrix}a_1,\ldots,a_p\\ b_1,\ldots,b_q\end{matrix}\right) = \mathrm{G}_{p\,q}^{m\,n}\left(x\,\middle|\,\begin{matrix}a_1+r,\ldots,a_p+r\\ b_1+r,\ldots,b_q+r\end{matrix}\right). \tag{29}$$

Moreover, it also employs the following definite integral (Gradshteyn and Ryzhik 2015, p. 861):

$$\int_0^\infty \exp(-\beta x)\,\mathrm{G}_{p\,q}^{m\,n}\left(\lambda x^2\,\middle|\,\begin{matrix}a_1,\ldots,a_p\\ b_1,\ldots,b_q\end{matrix}\right)dx = \frac{1}{\beta\sqrt{\pi}}\,\mathrm{G}_{p+2\,q}^{m\,n+2}\left(\frac{4\lambda}{\beta^2}\,\middle|\,\begin{matrix}0, \frac{1}{2}, a_1,\ldots,a_p\\ b_1,\ldots,b_q\end{matrix}\right). \tag{30}$$

C. Probability Density Function of Standardised Generalised Variance under Inverse Gamma Texture Model

Under the inverse gamma texture model, the texture component t is distributed as in (15) and the PDF of $\sqrt{|\mathbf{C}|}$ is given in (7). Since both the variables t and $\sqrt{|\mathbf{C}|}$ are statistically independent, their joint PDF is given by

$$f(t,\sqrt{|\mathbf{C}|}) = \frac{2L^2\alpha^{\alpha+1}}{\Gamma(\alpha+1)\,\Gamma(L-1)\,\Gamma(L)}\,t^{-\alpha-2}\,\frac{\sqrt{|\mathbf{C}|}}{|\boldsymbol{\Sigma}|}\exp(-\alpha/t)\,\mathrm{G}_{02}^{20}\left(L^2\frac{|\mathbf{C}|}{|\boldsymbol{\Sigma}|}\,\middle|\,\begin{matrix}-\\ L-2, L-1\end{matrix}\right). \tag{31}$$

Let $u = t\sqrt{|\mathbf{C}|}$ and $v = 1/t$, then the Jacobian of the transformation is $1/v$ and their joint PDF is

$$f(u,v) = \frac{2L^2\alpha^{\alpha+1}}{\Gamma(\alpha+1)\,\Gamma(L-1)\,\Gamma(L)}\,\frac{u}{|\boldsymbol{\Sigma}|}\,v^{\alpha+2}\exp(-\alpha v)\,\mathrm{G}_{02}^{20}\left(\frac{L^2u^2}{|\boldsymbol{\Sigma}|}v^2\,\middle|\,\begin{matrix}-\\ L-2, L-1\end{matrix}\right). \tag{32}$$

Hence,

$$\begin{aligned} f(u) &= \frac{2L^2\alpha^{\alpha+1}}{\Gamma(\alpha+1)\,\Gamma(L-1)\,\Gamma(L)}\,\frac{u}{|\boldsymbol{\Sigma}|}\int_0^\infty v^{\alpha+2}\exp(-\alpha v)\,\mathrm{G}_{02}^{20}\left(\frac{L^2u^2}{|\boldsymbol{\Sigma}|}v^2\,\middle|\,\begin{matrix}-\\ L-2, L-1\end{matrix}\right)dv \\ &= \frac{2\alpha^\alpha}{L^\alpha\,\Gamma(\alpha)\,\Gamma(L-1)\,\Gamma(L)}\,\frac{|\boldsymbol{\Sigma}|^{\alpha/2}}{u^{\alpha+1}}\int_0^\infty \exp(-\alpha v)\,\mathrm{G}_{02}^{20}\left(\frac{L^2u^2}{|\boldsymbol{\Sigma}|}v^2\,\middle|\,\begin{matrix}-\\ L+\frac{\alpha}{2}-1, L+\frac{\alpha}{2}\end{matrix}\right)dv \\ &= \frac{2\alpha^\alpha}{\sqrt{\pi}\,L^\alpha\,\Gamma(\alpha+1)\,\Gamma(L-1)\,\Gamma(L)}\,\frac{|\boldsymbol{\Sigma}|^{\alpha/2}}{u^{\alpha+1}}\,\mathrm{G}_{22}^{22}\left(\frac{4L^2u^2}{\alpha^2\,|\boldsymbol{\Sigma}|}\,\middle|\,\begin{matrix}0, \frac{1}{2}\\ L+\frac{\alpha}{2}-1, L+\frac{\alpha}{2}\end{matrix}\right). \end{aligned} \tag{33}$$

Note that the above solution uses (29) and (30).

D. Probability Density Function of Standardised Generalised Variance under Inverted Beta Texture Model

Under the inverted beta texture model, the texture component *t* is distributed as in (18) and the PDF of $\sqrt{|\mathbf{C}|}$ is given in (7). Since both the variables *t* and $\sqrt{|\mathbf{C}|}$ are statistically independent, their joint PDF is given by

$$f(t,\sqrt{|\mathbf{C}|}) = \frac{2L^2\Gamma(2\alpha+1)}{\Gamma(\alpha)\,\Gamma(\alpha+1)\,\Gamma(L-1)\,\Gamma(L)}\, t^{\alpha-1}(t+1)^{-2\alpha-1}\,\frac{\sqrt{|\mathbf{C}|}}{|\mathbf{\Sigma}|}\,\mathrm{G}_{02}^{20}\left(L^2\,\frac{|\mathbf{C}|}{|\mathbf{\Sigma}|}\,\middle|\,\begin{matrix}-\\ L-2, L-1\end{matrix}\right). \tag{34}$$

Let $u = t\sqrt{|\mathbf{C}|}$ and *v* = *t*, then the Jacobian of the transformation is 1/*v* and their joint PDF is

$$f(u,v) = \frac{2L^2\Gamma(2\alpha+1)}{\Gamma(\alpha)\,\Gamma(\alpha+1)\,\Gamma(L-1)\,\Gamma(L)}\,\frac{u}{|\mathbf{\Sigma}|}\,v^{\alpha-3}(v+1)^{-2\alpha-1}\,\mathrm{G}_{02}^{20}\left(\frac{L^2u^2}{|\mathbf{\Sigma}|\,v^2}\,\middle|\,\begin{matrix}-\\ L-2, L-1\end{matrix}\right). \tag{35}$$

Thus,

$$\begin{aligned} f(u) &= \frac{2L^2\Gamma(2\alpha+1)}{\Gamma(\alpha)\,\Gamma(\alpha+1)\,\Gamma(L-1)\,\Gamma(L)}\,\frac{u}{|\mathbf{\Sigma}|}\int_0^\infty v^{\alpha-3}(v+1)^{-2\alpha-1}\,\mathrm{G}_{20}^{02}\left(\frac{|\mathbf{\Sigma}|\,v^2}{L^2u^2}\,\middle|\,\begin{matrix}3-L, 2-L\\ -\end{matrix}\right)dv \\ &= \frac{4^\alpha L^2}{\pi\,\Gamma(\alpha)\,\Gamma(\alpha+1)\,\Gamma(L-1)\,\Gamma(L)}\,\frac{u}{|\mathbf{\Sigma}|}\,\mathrm{G}_{42}^{24}\left(\frac{|\mathbf{\Sigma}|}{L^2u^2}\,\middle|\,\begin{matrix}\frac{3}{2}-\frac{\alpha}{2}, 2-\frac{\alpha}{2}, 3-L, 2-L\\ \frac{3}{2}+\frac{\alpha}{2}, 2+\frac{\alpha}{2}\end{matrix}\right) \\ &= \frac{4^\alpha L^2}{\pi\,\Gamma(\alpha)\,\Gamma(\alpha+1)\,\Gamma(L-1)\,\Gamma(L)}\,\frac{u}{|\mathbf{\Sigma}|}\,\mathrm{G}_{24}^{42}\left(\frac{L^2u^2}{|\mathbf{\Sigma}|}\,\middle|\,\begin{matrix}-\frac{\alpha}{2}-\frac{1}{2}, -\frac{\alpha}{2}-1\\ \frac{\alpha}{2}-\frac{1}{2}, \frac{\alpha}{2}-1, L-2, L-1\end{matrix}\right). \end{aligned} \tag{36}$$

The above solution employs (28) and the following definite integral (Prudnikov *et al*. 1990, p. 348):

$$\int_0^\infty \frac{x^{\beta-1}}{(x+1)^\lambda}\,\mathrm{G}_{p\,q}^{m\,n}\left(\gamma x^2\,\middle|\,\begin{matrix}a_1,\ldots,a_p\\ b_1,\ldots,b_q\end{matrix}\right)dx = \frac{2^{\lambda-2}}{\pi\,\Gamma(\lambda)}\,\mathrm{G}_{p+2\,q+2}^{m+2\,n+2}\left(\gamma\,\middle|\,\begin{matrix}\frac{1}{2}-\frac{\beta}{2}, 1-\frac{\beta}{2}, a_1,\ldots,a_p\\ \frac{\lambda-\beta}{2}, \frac{\lambda-\beta+1}{2}, b_1,\ldots,b_q\end{matrix}\right). \tag{37}$$

REFERENCES

Anastassopoulos, V., Lampropoulos, G. A., Drosopoulos, A., and Rey, M. (1999). High resolution radar clutter statistics. *IEEE Transactions on Aerospace and Electronic Systems*, 35(1), pp. 43–60.

Anderson, T. W. (2003). *An Introduction to Multivariate Statistical Analysis*. 3rd ed., John Wiley & Sons, New York.

Andrews, L. C. (1998). *Special Functions of Mathematics for Engineers*. 2nd ed., SPIE, Washington.

Bagai, O. P. (1962). Distribution of the determinant of the sum of products matrix in the non-central linear case for some values of *p*. *Sankhya A*, 24(1), pp. 55–62.

Bagai, O. P. (1965). The distribution of the generalized variance. *The Annals of Mathematical Statistics*, 36(1), pp. 120–130.

Bian, Y. and Mercer, B. (2014). Multilook polarimetric SAR data probability density function estimation using a generalized form of multivariate K-distribution. *Remote Sensing Letters*, 5(7), pp. 682–691.

Consul, P. C. (1964). Distribution of the determinant of the sum of products matrix in the non-central linear case. *Mathematische Nachrichten*, 28(3-4), pp. 169–179.

Delignon, Y. and Pieczynski, W. (2002). Modeling non-Rayleigh speckle distribution in SAR images. *IEEE Transactions on Geoscience and Remote Sensing*, 40(6), pp. 1430–1435.

Erdélyi, A., Magnus, W., Oberhettinger, F., and Tricomi, F. G. (1953). *Higher Transcendental Functions – Volume I*. McGraw-Hill, New York.

Freitas, C. C., Frery, A. C., and Correia, A. H. (2005). The polarimetric G distribution for SAR data analysis. *Environmetrics*, 16, pp. 13–31.

Frery, A. C., Müller, H.-J., Yanasse, C. da C. F., and Sant'Anna, S. J. S. (1997). A model for extremely heterogeneous clutter. *IEEE Transactions on Geoscience and Remote Sensing*, 35(3), pp. 648–659.

Goodman, M. M. (1968). A measure of 'overall variability' in populations. *Biometrics*, 24(1), pp. 189–192.

Goodman, N. R. (1963). The distribution of the determinant of a complex Wishart distributed matrix. *The Annals of Mathematical Statistics*, 34(1), pp. 178–180.

Gradshteyn, I. S. and Ryzhik, I. M. (2015). *Table of Integrals, Series, and Products*. 8th ed., Elsevier, Amsterdam.

Gupta, A. K. and Rathie, P. N. (1983). On the noncentral distribution of the determinant of a complex Wishart matrix. *Metron*, 83(3-4), pp. 109–116.

Kocherlakota, S. and Kocherlakota, K. (1983). Generalized variance. In: *Encyclopedia of Statistical Sciences*, edited by Kotz, S., Johnson, N. L., and Read, C. B., vol. 3, John Wiley & Sons, New York, pp. 354–357.

Lee, J. S., Schuler, D. L., Lang, R. H., and Ranson, K. J. (1994). K-distribution for multi-look processed polarimetric SAR imagery. *Proceedings of the IEEE Geoscience and Remote Sensing Symposium*, vol. 4, pp. 2179–2181.

Lee, K. Y. and Bretschneider, T. B. (2013). Statistical modelling of sea clutter in airborne S-band fully polarimetric synthetic aperture radar imagery. *Proceedings of the Asian Conference on Remote Sensing*, paper no. SC01-0126.

Lee, K. Y. and Bretschneider, T. B. (2015). Clutter statistics in high-resolution synthetic aperture radar imagery. *Proceedings of the IEEE Geoscience and Remote Sensing Symposium*, pp. 1825–1828.

Luke, Y. L. (1969). *The Special Functions and Their Approximations – Volume I*. Academic Press, New York.

Mathai, A. M. (1970). Statistical theory of distributions and Meijer's G-function. *Metron*, 28(1-4), pp. 122–146.

Mathai, A. M. (1972). The exact non-central distribution of the generalized variance. *Annals of the Institute of Statistical Mathematics*, 24(1), pp. 53–65.

Mathai, A. M. and Rathie, P. N. (1971). The exact distribution of Wilks' generalized variance in the non-central linear case. *Sankhya A*, 33(1), pp. 45–60.

Mathai, A. M. and Saxena, R. K. (1973). *Generalized Hypergeometric Functions with Applications in Statistics and Physical Sciences*. Springer-Verlag, Berlin.

Moser, G., Zerubia, J., and Serpico, S. B. (2006). SAR amplitude probability density function estimation based on a generalized Gaussian model. *IEEE Transactions on Image Processing*, 15(6), pp. 1429–1442.

Prudnikov, A. P., Brychkov, Yu. A., and Marichev, O. I. (1990). *Integrals and Series – Volume 3: More Special Functions*. Gordon and Breach, New York.

Rencher, A. C. and Christensen, W. F. (2012). *Methods of Multivariate Analysis*. 3rd ed., John Wiley & Sons, New Jersey.

Sayama, S. and Sekine, M. (2002). Log-normal, log-Weibull and K-distributed sea clutter. *IEICE Transactions on Communications*, E85-B(7), pp. 1375–1381.

SenGupta, A. (1987a). Generalizations of Bartlett's and Hartley's tests of homogeneity using "overall variability". *Communications in Statistics – Theory and Methods*, 16(4), pp. 987–996.

SenGupta, A. (1987b). Tests for standardized generalized variances of multivariate normal populations of possibly different dimensions. *Journal of Multivariate Analysis*, 23, pp. 209–219.

SenGupta, A. (2006). Generalized variance. In: *Encyclopedia of Statistical Sciences*, edited by Kotz, S., Balakrishnan, N., Read, C. B., and Vidakovic, B., 2nd ed., vol. 4, John Wiley & Sons, New Jersey, pp. 2743–2747.

Wilks, S. S. (1932). Certain generalizations in the analysis of variance. *Biometrika*, 24(3/4), pp. 471–494.

Yueh, S. H., Kong, J. A., Jao, J. K., Shin, R. T., Zebker, H. A., and Le Toan, T. (1991). K-distribution and multi-frequency polarimetric terrain radar clutter. *Journal of Electromagnetic Waves and Applications*, 5(1), pp. 1–15.

Zhu, Y., Kam, P.-Y., and Xin, Y. (2009). On the mutual information distribution of MIMO Rician fading channels. *IEEE Transactions on Communications*, 57(5), pp. 1453–1462.